

# How widespread are aromatic cycles in cold clouds?★

M. Agúndez<sup>1</sup>, N. Marcelino<sup>2,3</sup>, B. Tercero<sup>2,3</sup>, and J. Cernicharo<sup>1</sup>

<sup>1</sup> Instituto de Física Fundamental, CSIC, Calle Serrano 123, E-28006 Madrid, Spain  
e-mail: marcelino.agundez@csic.es

<sup>2</sup> Observatorio Astronómico Nacional, IGN, Calle Alfonso XII 3, E-28014 Madrid, Spain

<sup>3</sup> Observatorio de Yebes, IGN, Cerro de la Palera s/n, E-19141 Yebes, Guadalajara, Spain

Received; accepted

## ABSTRACT

We report the detection of large hydrocarbon cycles toward several cold dense clouds. We observed four sources (L1495B, Lupus-1A, L483, and L1527) in the Q band (31–50 GHz) using the Yebes 40m radiotelescope. Using the line stack technique, we find statistically significant evidence of benzonitrile ( $C_6H_5CN$ ) in L1495B, Lupus-1A, and L483 at the  $31.8\sigma$ ,  $15.0\sigma$ , and  $17.2\sigma$  levels, respectively, while there is no hint of  $C_6H_5CN$  in the fourth source, L1527. The column densities derived are in the range  $(1.8\text{--}4.0)\times 10^{12}\text{ cm}^{-2}$ , which is somewhat below the value derived toward the cold dense cloud TMC-1. When we analyse together all the benzonitrile abundances derived toward cold clouds in this study and in the literature, a clear trend emerges in which the higher the abundance of  $HC_7N$ , the more abundant  $C_6H_5CN$  is. This indicates that aromatic cycles are specially favored in those interstellar clouds where long carbon chains are abundant, which suggests that the chemical processes that are responsible for the formation of linear carbon chains are also behind the synthesis of aromatic rings. We also searched for cycles other than benzonitrile, and found evidence of indene ( $C_9H_8$ ), cyclopentadiene ( $C_5H_6$ ), and 1-cyano cyclopentadiene ( $1\text{-}C_5H_5CN$ ) at the  $9.3\sigma$ ,  $7.5\sigma$ , and  $8.4\sigma$ , respectively, toward L1495B, which shows the strongest signal from  $C_6H_5CN$ . The relative abundances between the various cycles detected in L1495B are consistent, within a factor of three, to those found previously in TMC-1. It is therefore likely that not only  $C_6H_5CN$  but also other large aromatic cycles are abundant in clouds rich in carbon chains.

**Key words.** astrochemistry – line: identification – ISM: molecules – radio lines: ISM

## 1. Introduction

Cold dense clouds, with temperatures around 10 K and volume densities of a few  $10^4$  molecules of  $H_2$  per  $cm^3$  (Bergin & Tafalla 2007), are known to contain a rich variety of molecules, most of which are organic in nature. The chemical composition of this kind of environments has been long thought to be dominated by linear unsaturated carbon chains with a backbone of alternating triple and single bonds, such as polyynes and cyanopolyynes. Chemical models have been developed to explain the formation of molecules in these clouds, and they are reasonably successful in accounting for the abundances of the carbon chains observed in TMC-1, which is the paradigm of cold dense cloud rich in carbon chains (Agúndez & Wakelam 2013). The quest for chemical complexity in these clouds has been during years focused on the search for increasingly long linear chains, the largest one found to date being  $HC_{11}N$  (Loomis et al. 2021).

In recent years however we have experienced a change of paradigm concerning the chemistry of cold dense clouds. Large hydrocarbon cycles, some of them with aromatic character, have been discovered in TMC-1 by means of radioastronomical techniques. The first such molecule detected was benzonitrile ( $C_6H_5CN$ ; McGuire et al. 2018), which is the CN derivative of benzene ( $C_6H_6$ ) and is thought to be a proxy of the radioastronomically invisible aromatic molecule  $C_6H_6$  (Cooke et al. 2020). Also the CCH derivative of benzene ( $C_6H_5CCH$ ) has been iden-

tified toward TMC-1 (Cernicharo et al. 2021c; Loru et al. 2023), and the six-membered ring benzyne ( $C_6H_4$ ) has been also observed (Cernicharo et al. 2021b).

The five-membered ring cyclopentadiene ( $C_5H_6$ ), which is non aromatic but moderately polar, has been directly observed toward TMC-1 (Cernicharo et al. 2021a). In addition, the two CN isomeric derivatives (McCarthy et al. 2021; Lee et al. 2021) and the two CCH substituted isomers (Cernicharo et al. 2021c) have been detected. Moreover, fulvenallene ( $C_5H_4CCH_2$ ), which is also a derivative of cyclopentadiene, has been observed as well (Cernicharo et al. 2022).

In addition to single cycles, hydrocarbons composed of fused rings have been also detected toward TMC-1. The two simplest members of the family of polycyclic aromatic hydrocarbons, indene ( $C_9H_8$ ) and naphthalene ( $C_{10}H_8$ ), have been detected, either directly or indirectly. The non zero, although small, dipole moment of indene allowed for its detection (Cernicharo et al. 2021a; Burkhardt et al. 2021a), while one of the CN substituted isomers of indene was also detected (Sita et al. 2022). Naphthalene is non polar and thus cannot be observed through radioastronomical techniques, although the two CN substituted isomers have been observed (McGuire et al. 2021) which, similarly to the case of benzene, can be considered as proxies of naphthalene itself.

The observation of large cycles in cold dense clouds is challenging and thus has been restricted to TMC-1. In a recent study, Burkhardt et al. (2021b) reported the detection of  $C_6H_5CN$  toward four additional clouds. There are still many open questions regarding the presence of large hydrocarbon cycles in cold dense clouds, such as under which circumstances is their presence favored or how are they synthesized. Here we report the detec-

★ Based on observations carried out with the Yebes 40m telescope (projects 20A016, 21A006, and 22B023). The 40m radio telescope at Yebes Observatory is operated by the Spanish Geographic Institute (IGN; Ministerio de Transportes, Movilidad y Agenda Urbana).

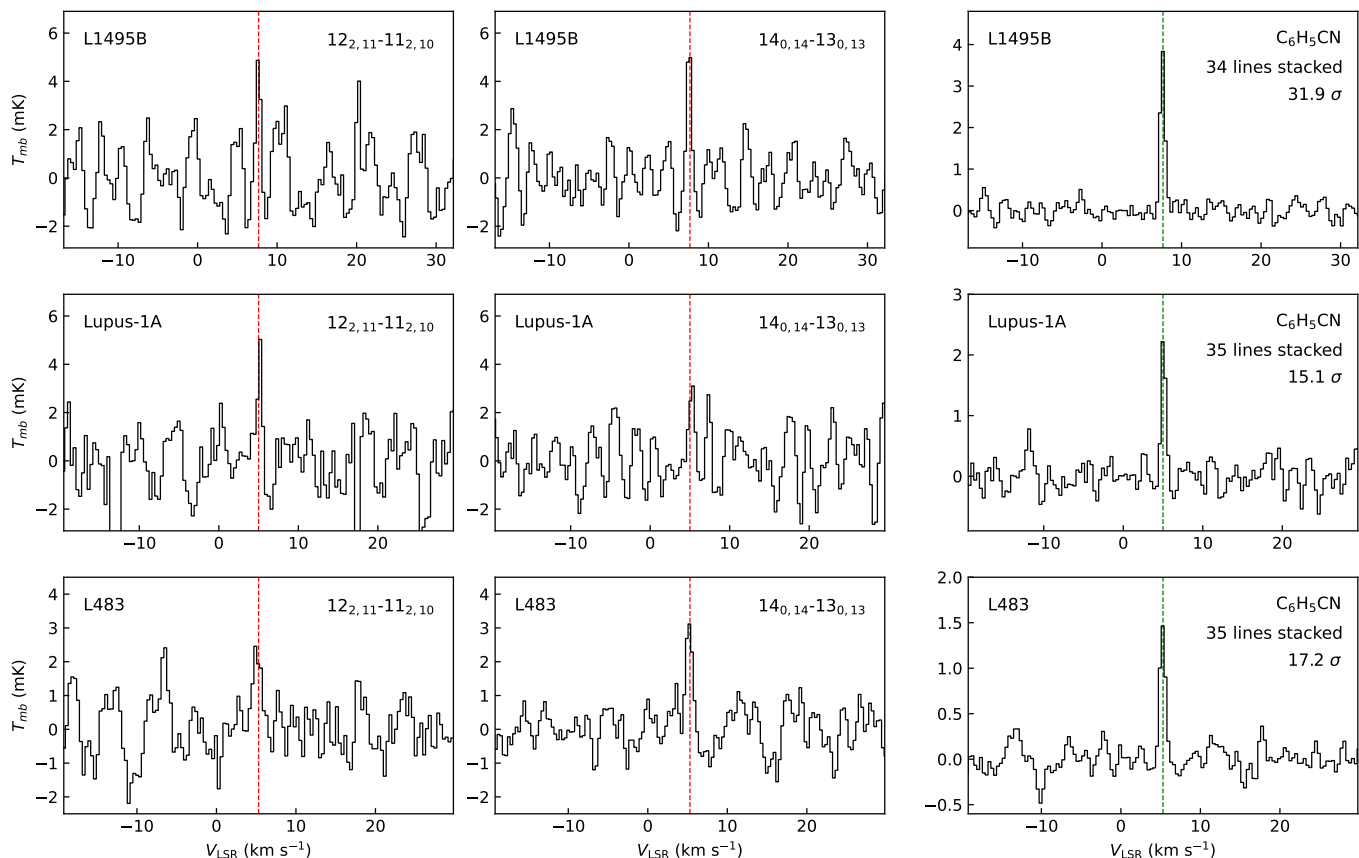


**Fig. 1.** Two individual lines of  $C_6H_5CN$  (left and middle panels) and stacked spectrum of  $C_6H_5CN$  (right panels) for L1495B (top row), Lupus-1A (middle row), and L483 (bottom row), using as reference line the  $13_{0,13}-12_{0,12}$  at 32833.813 MHz. The number of stacked lines and the significance level of the line stack signal (in units of  $\sigma$ ) is indicated in the right panels. The systemic velocity of each source is indicated by a vertical dotted line.

tion of large cycles toward new sources, which allows to build a larger statistical basis to understand the occurrence of large hydrocarbon cycles in cold interstellar clouds.

## 2. Astronomical observations

We carried out observations of four cold dense clouds (L1495B, Lupus-1A, L483, and L1527) with the Yebes 40m telescope in the frame of a line survey in the Q band and a search for negative ions (details and source coordinates are given in Agúndez et al. 2023). The observations, which used the 7 mm receiver described in Tercero et al. (2021), were taken between July 2020 and February 2023. The data consist of a full spectrum across the Q band (31.08-49.52 GHz) in horizontal and vertical polarizations with a spectral resolution of 38 kHz.

The observations were done using the frequency-switching technique. The frequency throw adopted, which changed between different observing periods as a result of tests done at the 40m telescope, was 10.52 MHz for L1495B and Lupus-1A, 10 MHz and 10.52 MHz for L483, and 8 MHz for L1527. We used two spectral setups with the frequency of the local oscillator separated by 5 MHz to identify spurious signals. Total on-source telescope times in each polarization were 45 h for L1495B, 120 h for Lupus-1A, 103 h for L483, and 40 h for L1527. The intensity scale at the 40m telescope is antenna temperature,  $T_A^*$ , for which we estimate a calibration error of 10 %.

The  $T_A^*$  noise levels, after averaging horizontal and vertical polarizations, are in the range 0.8-2.6 mK for L1495B, 0.7-2.8 mK for Lupus-1A, 0.4-1.0 mK for L483, and 0.7-2.7 mK for L1527. We convert  $T_A^*$  to  $T_{mb}$  (main beam brightness temperature) by dividing by  $B_{eff}/F_{eff}$ , where for the 40m telescope in the Q band  $B_{eff} = 0.797 \exp[-(\nu(\text{GHz})/71.1)^2]$  and  $F_{eff} = 0.97$ . The half power beam width (HPBW) can be fitted as a function of frequency as  $HPBW('') = 1763/\nu(\text{GHz})$ .

## 3. Detection by line stack

The Yebes 40m data of the L1495B, Lupus-1A, L483, and L1527 were analyzed using the program CLASS of the GILDAS software (Pety 2005)<sup>1</sup>. While inspecting the data we noticed the presence of several individual lines of  $C_6H_5CN$  in the spectrum of L1495B. The lines were weak, with  $T_{mb} \sim 2-5$  mK (see left panels in the top row in Fig. 1). We also searched for  $C_6H_5CN$  in the spectra of Lupus-1A and L483, although we only found a few lines barely visible above the noise level (see left panels in the middle and bottom rows in Fig. 1), while many others were hidden within the noise. In the case of L1527 no obvious line of  $C_6H_5CN$  was seen. Given that benzonitrile has many lines with similar intensities within the Q band, as seen in the very sensitive spectrum of TMC-1 (Cernicharo et al. 2021c), we decided to use the line stack technique to evaluate whether or not there

<sup>1</sup> <https://www.iram.fr/IRAMFR/GILDAS/>

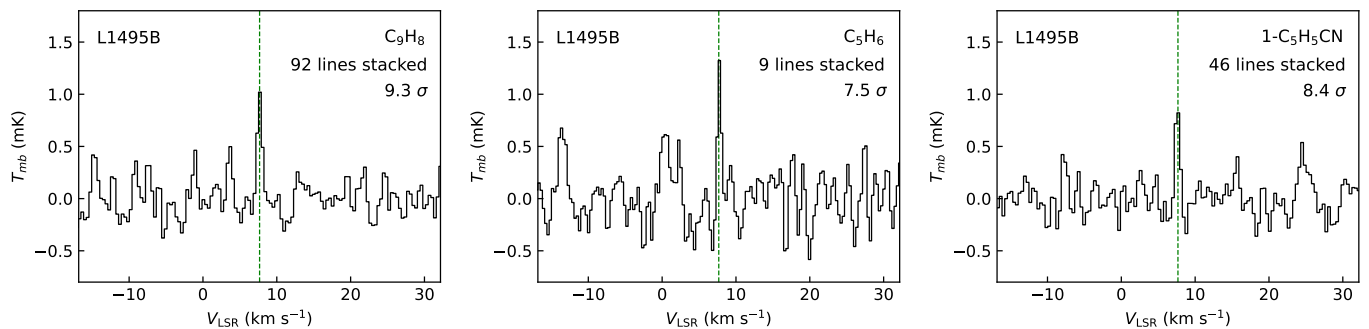


**Fig. 2.** Stacked spectra of L1495B for  $C_9H_8$  (left panel),  $C_5H_6$  (middle panel), and  $1-C_5H_5CN$  (right panel), using as reference line the  $14_{0,14}-13_{0,13}$  at 32528.329 MHz,  $3_{1,2}-2_{2,1}$  at 37453.992 MHz, and  $10_{0,10}-9_{0,9}$  at 33050.464 MHz, respectively. The number of stacked lines and the significance level of the line stack signal (in units of  $\sigma$ ) is indicated in each panel. The systemic velocity of L1495B is indicated by a vertical dotted line.

is spectral evidence of this molecule in the four aforementioned sources.

In order to carry out the line stack we restricted to the most intense lines of  $C_6H_5CN$  in the Q band, which are those with quantum number  $K_a = 0, 1, 2$  in Figs. C.1-C.4 of Cernicharo et al. (2021c) (35 lines in total). The hyperfine splitting of these lines is small (10-30 kHz). Lines with  $K_a > 2$  are weaker and have significant hyperfine splitting, which further dilutes the intensity among the different hyperfine components (see spectrum of TMC-1 in Cernicharo et al. 2021c). The line frequencies and strengths of benzonitrile were computed from the rotational constants and dipole moments reported by Wohlfart et al. (2008). We selected a spectral region of  $\pm 30 \text{ km s}^{-1}$  around each line and cleaned the channels belonging to spectral features other than the  $C_6H_5CN$  target line, i.e., lines from other molecules, negative frequency-switching artifacts, or spurious signals. In order to take into account the different expected intensities of the lines under consideration, we computed the spectrum under local thermodynamic equilibrium (LTE) at a temperature of 10 K. We note that the only determination of the rotational temperature of  $C_6H_5CN$  reported in the literature, which corresponds to TMC-1 (Cernicharo et al. 2021c), yields a value of 9 K, which is equal to the gas kinetic temperature in this source (Agúndez et al. 2023). Benzonitrile is therefore likely to be thermalized in cold dense clouds. The gas kinetic temperature is around 10 K in the four studied sources (Agúndez et al. 2023), and therefore we adopt this round value here for simplicity. We arbitrarily selected as reference the  $13_{0,13}-12_{0,12}$  line at 32833.813 MHz and used the calculated brightness temperatures of the LTE spectrum to compute relative intensities with respect to the reference line. We then scaled the spectrum of each line by the inverse of the theoretical relative intensity.

Once we have each spectrum cleaned from signals other than the target  $C_6H_5CN$  line and conveniently scaled according to the expected relative intensity, we fitted a baseline to a polynomial of degree 10 (the frequency-switching technique produces baseline ripples) and subtracted it. We then stacked all spectra aligned in the velocity scale using as weight the inverse square of the rms noise level. The line stack procedure used here, which is similar to that employed to map  $C_6H_5CN$  in TMC-1 (Cernicharo et al. 2023), has two benefits. On the one hand, it controls the absolute scale of the intensity since all lines are stacked with the same intensity of that of the reference line. Therefore, the intensity of the signal after the line stack can be assigned to the reference line, which permits a correct evaluation of the column density. On the other hand, lines contribute to the signal according to their expected relative intensities. That is, the weaker the line,

the higher the factor by which the spectrum is multiplied, the higher the noise level, and the lower the weight. This way, we avoid that weak lines dilute the line stack signal.

The results from the line stack of  $C_6H_5CN$  are shown in the right panels of Fig. 1 for L1495B, Lupus-1A, and L483. In the three cases there is a clear signal, well above the noise level and precisely centered at the systemic velocity of each source,  $7.67 \text{ km s}^{-1}$  for L1495B (Cordiner et al. 2013; Agúndez et al. 2023),  $5.00 \text{ km s}^{-1}$  for Lupus-1A (Sakai et al. 2010), and  $5.30 \text{ km s}^{-1}$  for L483 (Agúndez et al. 2019). We note that in the case of L1495B, we removed one line from the analysis because it overlaps with a spurious signal. The signal-to-noise ratio (S/N) is evaluated as  $\int T_A^* dv / [\text{rms} \times \sqrt{\Delta v \times \delta v}]$ , where rms is the measured noise level of the stacked spectrum,  $\delta v$  is the spectral resolution in velocity of the stacked spectrum, and  $\int T_A^* dv$  and  $\Delta v$  are the velocity-integrated intensity and full width at half maximum, respectively, given by a Gaussian fit to the line profile. Given the limitations associated to the line stack procedure, we consider that a detection is statistically significant when the S/N is above  $5\sigma$ . We carried out the same line stack analysis to search for evidence of  $C_6H_5CN$  in L1527, although no statistically significant signal was detected. The non detection of  $C_6H_5CN$  in L1527 allows to impose a stringent upper limit to the column density of  $C_6H_5CN$ . This is interesting because L1527 is known to be rich in carbon chains (Sakai et al. 2008).

Motivated by the detection of benzonitrile in the three clouds L1495B, Lupus-1A, and L483, we searched for evidence of other large cycles in these sources. Guided by previous observations toward TMC-1 (Cernicharo et al. 2021a,c; McGuire et al. 2021), we searched for cyclopentadiene and its CN and CCH derivatives, for indene, and for the CN derivatives of naphthalene. For all these molecules, we computed the LTE spectrum at 10 K, arbitrarily selected as reference one intense line (see caption of Fig. 2), and evaluated the relative line intensities from the calculated brightness temperatures. We only included those lines that are calculated to have at least the intensity of the reference line. The line frequencies and strengths were computed from the rotational constants and dipole moments reported in the literature:  $C_5H_6$  (Bogey et al. 1988; Laurie 1956), 1- and 2- $C_5H_5CN$  (Cernicharo et al. 2021c; Sakaizumi et al. 1987), 1- and 2- $C_5H_5CCH$  (Cernicharo et al. 2021c),  $C_9H_8$  (Cernicharo et al. 2021a; Caminati 1993), and 1- and 2- $C_{10}H_7CN$  (McNaughton et al. 2018). We then carried out the line stack analysis in exactly the same manner employed for  $C_6H_5CN$ . We found a line stack signal statistically significant for indene, cyclopentadiene, and 1- $C_5H_5CN$  in the L1495B cloud. The stacked spectra are shown in Fig. 2, where we also give the number of lines included

**Table 1.** Observed column densities.

Molecule	Source	$T_{\text{rot}}^a$ (K)	$N$ ( $\text{cm}^{-2}$ )
$\text{C}_6\text{H}_5\text{CN}$	L1495B		$3.8 \times 10^{11}$
$\text{C}_6\text{H}_5\text{CN}$	Lupus-1A		$2.1 \times 10^{11}$
$\text{C}_6\text{H}_5\text{CN}$	L483		$1.7 \times 10^{11}$
$\text{C}_6\text{H}_5\text{CN}$	L1527		$<6.5 \times 10^{10}{}^b$
$\text{C}_9\text{H}_8$	L1495B		$1.1 \times 10^{13}$
$\text{C}_5\text{H}_6$	L1495B		$7.8 \times 10^{12}$
$1\text{-C}_5\text{H}_5\text{CN}$	L1495B		$6.6 \times 10^{10}$
$\text{HC}_7\text{N}$	L1495B	$9.3 \pm 0.4$	$(2.7 \pm 0.4) \times 10^{12}$
$\text{HC}_7\text{N}$	Lupus-1A	$9.7 \pm 0.4$	$(6.3 \pm 0.9) \times 10^{12}$
$\text{HC}_7\text{N}$	L483	$11.1 \pm 0.4$	$(2.2 \pm 0.3) \times 10^{12}$
$\text{HC}_7\text{N}$	L1527	$17.0 \pm 1.2$	$(7.4 \pm 1.2) \times 10^{11}$

<sup>a</sup> The rotational temperature for the cycles detected through line stack is assumed to be 10 K in all sources.

<sup>b</sup> Upper limit calculated at the  $5\sigma$  level.

in the line stack analysis and the S/N reached. The significance levels are well above the  $5\sigma$  threshold. In any case we plan to perform new observations of L1495B to provide a more robust identification of these three cycles and to search for other cycles not yet detected. The detection of these three particular cycles in L1495B is consistent with (1) the fact that this is the cloud with the highest signal of  $\text{C}_6\text{H}_5\text{CN}$  among the sources studied here, and (2) the relative intensities of the different cycles observed in TMC-1. In this regard, it makes sense that the only derivative of cyclopentadiene detected in L1495B is  $1\text{-C}_5\text{H}_5\text{CN}$  because this is the one showing the higher line intensities in TMC-1 (Cernicharo et al. 2021c). We also note that in the case of the CN derivatives of naphthalene, the search would be better carried out at frequencies below 30 GHz because of the small rotational constants.

#### 4. Discussion

To compute column densities for the cycles detected through line stack we assumed that the velocity-integrated intensity of the stacked line corresponds to the reference line and adopted a round value of 10 K for the rotational temperature. The column densities derived are given in Table 1. In the case of L1527, we derived a  $5\sigma$  upper limit to the column density of  $\text{C}_6\text{H}_5\text{CN}$ .

Benzonitrile is the aromatic cycle that has been most widely observed in cold dense clouds. In addition to the detection in TMC-1 (McGuire et al. 2018; Cernicharo et al. 2021c), it has been also observed in four other cold clouds (Burkhardt et al. 2021b), three clumps in the Serpens South star-forming region (named 1a, 1b, and 2; Friesen et al. 2013), and in the L1521F core, located in the Taurus Molecular Cloud region (Crapsi et al. 2004). In their study, Burkhardt et al. (2021b) find that the abundance of benzonitrile relative to  $\text{HC}_7\text{N}$  varies considerably between the Taurus and Serpens sources. Concretely, the abundance ratio  $\text{C}_6\text{H}_5\text{CN}/\text{HC}_7\text{N}$  is about four times higher in the Taurus clouds TMC-1 and L1521F compared to the three Serpens clouds. Here we report the detection of benzonitrile in three additional cold clouds and the non detection in a fourth one. Therefore, we have now a sizable sample of nine sources where benzonitrile has been detected, or at least searched for, to examine how does benzonitrile behaves among different cold clouds. The nine clouds have in common that they are rich in carbon chains. It is therefore interesting to evaluate whether the abundance of benzonitrile is linked to that of carbon chains. To this

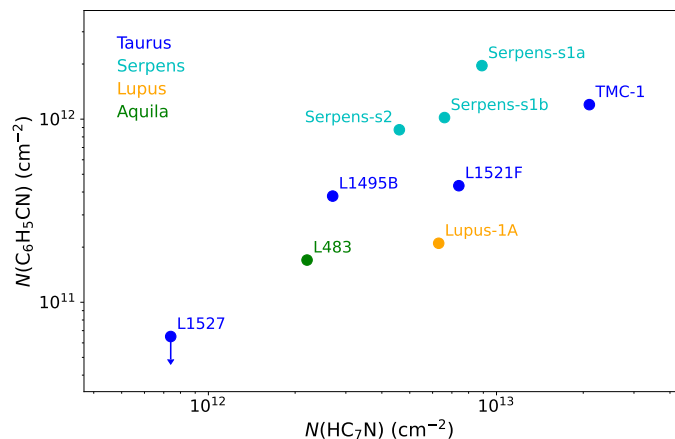


**Fig. 3.** Column density of  $\text{C}_6\text{H}_5\text{CN}$  versus column density of  $\text{HC}_7\text{N}$  for all the clouds where  $\text{C}_6\text{H}_5\text{CN}$  has been detected or searched for. The colors indicate different locations in the sky. Values were taken from Cabezas et al. (2022) and Cernicharo et al. (2021c) for TMC-1, from Friesen et al. (2013) and Burkhardt et al. (2021b) for the three clouds in Serpens and L1521F, and from this work elsewhere.

purpose, we calculated column densities for  $\text{HC}_7\text{N}$  in the four clouds studied here using our Yebes 40m data and the rotation diagram method. The calculated column densities, together with the rotational temperatures derived, are given in Table 1.

In Fig. 3 we represent the column densities of  $\text{C}_6\text{H}_5\text{CN}$  with respect to those of  $\text{HC}_7\text{N}$ . We can appreciate a very suggestive trend in which the higher the column density of  $\text{HC}_7\text{N}$ , the more abundant  $\text{C}_6\text{H}_5\text{CN}$  is. The L1527 data point, even if it only provides an upper limit to the column density of benzonitrile, brings a precious information supporting the positive correlation between aromatic cycles and linear chains. We can also see that the abundance of benzonitrile varies depending on the region where the cloud is located. For example, Serpens-s1a, Serpens-s1b, L1521F, and Lupus-1A have a similar column density of  $\text{HC}_7\text{N}$ , although the column density of  $\text{C}_6\text{H}_5\text{CN}$  varies considerably, with the two Serpens clouds having significantly higher abundances than Lupus-1A. Regarding the evolutionary status of the clouds, most sources in Fig. 3 do not contain a protostar, while L1521F hosts a very low luminosity object (Bourke et al. 2006), and L483 and L1527 are known to contain a protostar (Agúndez et al. 2019; Sakai et al. 2008). It is interesting to note that the two protostellar sources are the ones where benzonitrile is less abundant, although it is also true that these two clouds have low column densities of  $\text{HC}_7\text{N}$ , compared to the rest of sources. It thus appear that aromatic cycles are favored in those clouds where carbon chains are abundant, which tend to be associated with early evolutionary stages along the process of star formation. The relationship between aromatic cycles and carbon chains is strengthened by the fact that the spatial distribution of  $\text{C}_6\text{H}_5\text{CN}$  in TMC-1 coincides with that of carbon chains, such as  $\text{HC}_3\text{N}$ ,  $\text{HC}_5\text{N}$ ,  $\text{HC}_7\text{N}$ , and  $\text{C}_6\text{H}$  (Cernicharo et al. 2023).

Given that we have detected several large cycles in L1495B, it seems interesting to know whether or not the relative abundances between the various cycles are similar to those found in TMC-1. Indene is the only species composed of fused rings that has been detected in L1495B. According to the values given in Table 1, indene has an abundance 29 times higher than that of benzonitrile. This value is on the order of that found in TMC-1, where the abundance ratio  $\text{C}_9\text{H}_8/\text{C}_6\text{H}_5\text{CN}$  is 13 (Cernicharo et al. 2021a,c). It is also interesting to note that the column density

of indene in L1495B is on the same order than that of the single five-membered cycle cyclopentadiene (the  $C_9H_8/C_5H_6$  ratio is 1.4; see Table 1), while the same is also found in TMC-1, where the  $C_9H_8/C_5H_6$  abundance ratio is 1.3 (Cernicharo et al. 2021a). Finally, it is also interesting to examine the abundance ratio between a pure hydrocarbon cycle such as cyclopentadiene and its CN derivative. In L1495B, the abundance of the isomer 1- $C_5H_5CN$  is 0.8 % of that of  $C_5H_6$  (see Table 1), while in TMC-1 this isomer is present with abundance 2.6 % of that of cyclopentadiene. In summary, the abundance ratios between different cycles in L1495B are consistent with those found in TMC-1 within a factor of three.

The positive correlation between the abundance of  $C_6H_5CN$  and  $HC_7N$  found here, together with the coincident spatial distribution of benzonitrile and carbon chains found in TMC-1 by Cernicharo et al. (2023), suggest that there is a chemical link between aromatic cycles and carbon chains. That is, that the same kind of chemistry that is responsible for the formation of linear chains is also behind the synthesis of aromatic rings. However, while the synthesis of carbon chains can be explained by current gas-phase chemical models of cold dense clouds (e.g., Agúndez & Wakelam 2013), it is not yet well understood how large hydrocarbon cycles are formed in these environments.

While it is nowadays generally accepted that aromatic rings are formed in situ in the cold clouds where they are detected, there is still debate on which are the processes that drive the cyclization from small hydrocarbon species to single cycles such as cyclopentadiene and benzene. It has been proposed that benzene can be formed through ion-neutral reactions that lead to the  $C_6H_7^+$  ion (McEwan et al. 1999; Woods 2011; Agúndez et al. 2021), although there are important uncertainties, to name one the branching ratios of the dissociative recombination of the ion  $C_6H_7^+$  that is thought to lead to benzene. Some neutral-neutral reactions have been studied and are promising routes to cyclopentadiene and benzene in cold clouds. For example, the reaction between 1,3-butadiene and the radical CH can yield cyclopentadiene (He et al. 2020), which upon further reaction with CH can produce benzene (Caster et al. 2021). Benzene can also be formed in the reaction between  $C_2H$  and 1,3-butadiene (Jones et al. 2011). However, when this chemical scheme (see Appendix D in Cernicharo et al. 2021c) is implemented in chemical models of cold dense clouds, the calculated abundances of benzonitrile and cyclopentadiene fall below the observed values (Burkhardt et al. 2021b; Cernicharo et al. 2022). There are still many reactions that need to be studied before understanding how cyclization occurs in cold clouds. A recent example is the study of the reaction between the propargyl and vinyl radicals by García de la Concepción et al. (2023). Moreover, we also need to understand how single cycles such as cyclopentadiene and benzene convert into fused rings such as indene and naphthalene. In this context, Doddipatla et al. (2021) have recently found that indene can be formed in the reaction of vinyl benzene with CH.

In addition to the challenge of explaining how aromatic cycles are formed in cold clouds, constraining how abundant and widespread they are is interesting to evaluate their role in the physical and chemical evolution of the clouds. For example, cycles such as indene and naphthalene are little polar and have large sizes, which make them strong candidates to be deposited as ices on dust grains. In a recent study, Maté et al. (2023) find that the abundance of indene observed in TMC-1 implies that it should be present on ices with an exceedingly large abundance, accounting for up to 2 % of the carbon, which seems unrealistically high. It is clear that we still need to understand the interplay between gas and dust regarding these very big cycles. Astro-

nomical observations able to constrain the type of regions where aromatic rings are present and their abundances, combined with laboratory and theoretical studies, will eventually allow to reach a good understanding of the chemistry and physics of large aromatic rings in cold clouds.

## 5. Conclusions

We searched for large hydrocarbon cycles in four cold dense clouds. Using the line stack technique, we detected benzonitrile in three sources (L1495B, Lupus-1A, and L483), while it was not detected toward the fourth one (L1527). In addition we detected three other cycles, namely indene, cyclopentadiene, and 1-cyano cyclopentadiene, toward L1495B. By analyzing the abundances of benzonitrile derived here, together with values derived in the literature toward other sources, we find a positive correlation between the column density of  $C_6H_5CN$  and that of  $HC_7N$ . This result indicates that aromatic rings are favored in those regions where long carbon chains are abundant. The various cycles are likely to have similar relative abundances in cold dense clouds, as suggested by the comparison between L1495B and TMC-1.

*Acknowledgements.* We acknowledge funding support from Spanish Ministerio de Ciencia e Innovación through grants PID2019-106110GB-I00, PID2019-107115GB-C21, and PID2019-106235GB-I00. We thank the anonymous referee for a report that helped to improve this paper.

## References

- Agúndez, M. & Wakelam, V. 2013, *Chem. Rev.*, 113, 8710  
 Agúndez, M., Marcelino, N., Cernicharo, J., et al. 2019, *A&A*, 625, A147  
 Agúndez, M., Cabezas, C., Tercero, B., et al. 2021, *A&A*, 647, L10  
 Agúndez, M., Marcelino, N., Tercero, B., et al. 2023, *A&A*, in press; DOI: 10.1051/0004-6361/202347077; arXiv:2307.04487  
 Bergin, E. A. & Tafalla, M. 2007, *ARA&A*, 45, 339  
 Bogey, M., Demuynck, C. & Destombes, J. L. 1988, *J. Mol. Spectr.*, 132, 277  
 Bourke, T. L., Myers, P. C., Evans II, N. J., et al. 2006, *ApJ*, 649, L37  
 Burkhardt, A. M., Lee, K. L. K., Changala, P. B., et al. 2021a, *ApJ*, 913, L18  
 Burkhardt, A. M., Loomis, R. A., Shingledecker, C. N., et al. 2021b, *Nat. Astron.*, 5, 181  
 Cabezas, C., Agúndez, M., Marcelino, N., et al. 2022, *A&A*, 659, L8  
 Caminati, W. 1993, *J. Chem. Soc. Faraday Trans.*, 89, 4153  
 Caster, K. L., Selby, T. M., Osborn, D. L., et al. 2021, *J. Phys. Chem. A*, 125, 6927  
 Cernicharo, J., Agúndez, M., Cabezas, C., et al. 2021a, *A&A*, 649, L15  
 Cernicharo, J., Agúndez, M., Kaiser, R. I., et al. 2021b, *A&A*, 652, L9  
 Cernicharo, J., Agúndez, M., Kaiser, R. I., et al. 2021c, *A&A*, 655, L1  
 Cernicharo, J., Fuentetaja, R., Agúndez, M., et al. 2022, *A&A*, 663, L9  
 Cernicharo, J., Tercero, B., Marcelino, N., et al. 2023, *A&A*, 674, L4  
 Cooke, I. R., Gupta, D., Messinger, J. P., & Sims, I. R. 2020, *ApJ*, 891, L41  
 Cordiner, M. A., Buckle, J. V., Wirstrom, E. S., et al. 2013, *ApJ*, 770, 48  
 Crapsi, A., Caselli, P., Walmsley, C. M., et al. 2004, *A&A*, 420, 957  
 Doddipatla, S., Galimova, G. R., Wei, H., et al. 2021, *Sci. Adv.*, 7, eabd4044  
 Friesen, R. K., Medeiros, L., Schnee, S., et al. 2013, *MNRAS*, 436, 1513  
 García de la Concepción, J., Jiménez-Serra, I., Rivilla, V. M., et al. 2023, *A&A*, 673, A118  
 He, C., Zhao, L., Doddipatla, S., et al. 2020, *Chem. Phys. Chem.*, 21, 1295  
 Jones, B. M., Zhang, F., Kaiser, R. I., et al. 2011, *PNAS*, 108, 452  
 Laurie, V. M. 1956, *J. Chem. Phys.*, 24, 635  
 Lee, K. L. K., Changala, P. B., Loomis, R. A., et al. 2021, *ApJ*, 910, L2  
 Loomis, R. A., Burkhardt, A. M., Shingledecker, C. N., et al. 2021, *Nat. Astron.*, 5, 188  
 Loru, D., Cabezas, C., Cernicharo, J., et al. 2023, *A&A*, in press; DOI: 10.1051/0004-6361/202347023  
 Maté, B., Tanarro, I., Timón, V., et al. 2023, *MNRAS*, 523, 5887  
 McCarthy, M. C., Lee, K. L. K., Loomis, R. A., et al. 2021, *Nat. Astron.*, 5, 176  
 McEwan, M. J., Scott, G. B. I., Adams, N. G., et al. 1999, *ApJ*, 513, 287  
 McGuire, B. A., Burkhardt, A. M., Kalenskii, S., et al. 2018, *Science*, 359, 6372  
 McGuire, B. A., Loomis, R. A., Burkhardt, A. M., et al. 2021, *Science*, 371, 1265  
 McNaughton, D., Jahn, M. K., Travers, M. J., et al. 2018, *MNRAS*, 476, 5268  
 Pety, J. 2005, in *SF2A-2005: Semaine de l'Astrophysique Française*, ed. F. Casoli et al. (Les Ulis: EDP-Sciences), 721  
 Sakai, N., Sakai, T., Hirota, T., & Yamamoto, S. 2008, *ApJ*, 672, 371  
 Sakai, N., Shiino, T., Hirota, T., et al. 2010, *ApJ*, 718, L49  
 Sakaizumi, T., Kikuchi, H., Ohashi, O., & Yamaguchi, I. 1987, *Bull. Chem. Soc. Japan*, 60, 3903  
 Sita, M. L., Changala, P. B., Xue, C., et al. 2022, *ApJ*, 938, L12  
 Tercero, F., López-Pérez, J. A., Gallego, J. D., et al. 2021, *A&A*, 645, A37  
 Wohlhart, K., Schnell, M., Grabow, J.-U., & Küpper, J. 2008, *J. Mol. Spectr.*, 247, 119  
 Woods, P. M. 2011, in *EAS Publication Series*, 46, 235